

A multiplexed fiber Bragg grating sensor for simultaneous salinity and temperature measurement

Liqiu Men,¹ Ping Lu,¹ and Qiying Chen^{1,a)}

¹*Department of Physics and Physical Oceanography, Memorial University of Newfoundland, St. John's, Newfoundland A1B 3X7, Canada*

(Received 22 November 2007; accepted 29 December 2007; published online 11 March 2008)

An in-line one-fiber approach to realize simultaneous measurement of salinity and temperature is proposed. The sensor system, which consists of multiplexed polymer-coated fiber Bragg gratings, showed that the polyimide-coated grating responds to variations of both temperature and salinity, while the acrylate-coated grating is only sensitive to the environmental temperature. The experimental results indicated that the temperature sensitivity of the acrylate-coated grating in water was 0.0102 nm/°C for redshifted Bragg wavelength with increasing temperature, and the temperature and the salinity sensitivities of the polyimide-coated grating were 0.0094 nm/°C (redshifted) and 0.0165 nm/M (blueshifted), respectively, which are in excellent agreement with the theoretical analysis. © 2008 American Institute of Physics. [DOI: 10.1063/1.2890156]

I. INTRODUCTION

In situ monitoring of physical, chemical, and biological parameters is of great importance for process control in manufacturing industries, protection of ecosystems, and prevention of global warming.^{1,2} Salinity and temperature are the most important parameters in these applications, especially in physical oceanography.² Traditionally, the degree of salinity of water is determined by the measurement of electrical conductivity due to the presence of chlorine ions in the water solution.³ The standard optical technique to derive the information on salinity of a solution is to measure the optical refractive index through a refractometer, for which many well-known apparatus such as Pulfrich and Abbe refractometers have been used for many years.⁴ The refractometers, for its wide range of applications unbounded by the salinity measurement, had undergone constant improvement over years to have enhanced accuracy and low sensitivity to temperature,⁵ for example, differential-type⁶ and waveguide-type refractometers.⁷ Modern versions of refractometers used optical fibers to collect the refracted lights.^{6,8,9} However, only a few papers discussed the measurement of salinity by the use of these refractometers, which were essentially bulky prism systems.^{8,9}

In recent years, fiber-optic sensors have received great attention for their unique advantages such as immunity to electromagnetic interference, compact size, potential low cost, and the possibility of distributed measurement over a long distance.^{10,11} Fiber-optic sensors have been reported as powerful sensors for many measurands including temperature,¹² strain,¹³ displacement,¹⁴ velocity,¹⁵ gas,¹⁶ vacuum,¹⁷ ambience,¹⁸ and magnetic field.¹⁹ Esteban *et al.* reported the use of surface plasmon resonance in thin metallic films deposited on side-polished fibers to measure the attenuated power guided by a fiber in order to obtain the refractive index.³ The salinity of water was then derived

through an empirical algorithm. Gentleman *et al.* also discussed the salinity measurement by utilizing surface plasmon resonance with the fragile fiber tip removed of cladding and buffer as the sensing region, followed by polishing and coating of metallic Cr and Au layers at the fiber tip.²⁰ Falate *et al.* reported an approach to measure the refractive index based on a phase-shifted long-period fiber grating in order to derive the salinity of water empirically.²¹ Cong *et al.* reported a fiber-optic Bragg grating sensor based on hydrogels for measuring salinity, in which complicated processes were involved to fabricate a coating of monomer and photoinitiator with the insertion of special clamps inside the coating to form the fiber transducer.²²

In all these reported methods to measure the salinity, either bulky prism refractometer systems or fiber systems of complicated configurations and fabrication procedures had been adopted and the salinity was derived through empirical algorithms. Furthermore, as it is well known that the refractive index of water decreases with the temperature, it is necessary to realize simultaneous measurement of salinity and temperature in order to obtain an accurate value of salinity. In this paper, a new in-line one-fiber approach to realize simultaneous measurement of salinity and temperature is proposed and demonstrated. In our approach, polyimide and acrylate polymers, which possess excellent strength and resistance to breakage, are used as the coating materials for different fiber Bragg gratings (FBGs) in the sensor system. These polymer materials are innocuous and harmless to human beings and the environment. In order to achieve *in situ* measurement of these two parameters, our sensor system has been designed as a multiplexed system, in which an acrylate-coated FBG is not sensitive to the salinity and functions as a temperature sensor, while a polyimide-coated FBG measures the salinity. Theoretical analysis on the simultaneous measurement of salinity and temperature has been carried out to verify the experimental results.

^{a)}Author to whom correspondence should be addressed. Electronic mail: qiyingc@mun.ca.

TABLE I. Thermo-optic parameters of the fused silica fiber and the polyimide coating.

Parameter	Value	Ref
Thermal expansion coefficient α_f (K^{-1})	5×10^{-7}	25
Thermal expansion coefficient α_c (K^{-1})	4×10^{-5}	26
Thermo-optic coefficient ξ (K^{-1})	$(55 \pm 4.8) \times 10^{-7}$	27
Young's modulus E (fiber) (GPa)	72	28
Young's modulus E (coating) (GPa)	2.45	26
Poisson's ratio ν (fiber)	0.17	25
Poisson's ratio ν (coating)	0.41	26
Hygroscopic expansion coefficient β_f ($\%RH^{-1}$)	0	23
Hygroscopic expansion coefficient β_c ($\%RH^{-1}$)	7×10^{-5}	29
Thermal longitudinal expansion coefficient of coated fiber α_{cf} (K^{-1})	1.39×10^{-6}	23
Hygroscopic longitudinal expansion coefficient of coated fiber β_{cf} ($\%RH^{-1}$)	1.58×10^{-6}	23

II. THEORY

The Bragg resonance of a FBG, λ_B , which is the center wavelength of light backreflected from the grating, depends on the effective index of refraction of the core (n_{eff}) and the periodicity of the grating (Λ) through the relation $\lambda_B = 2n_{eff}\Lambda$. Parameters such as n_{eff} and Λ are affected by changes in strain and temperature. The shift in the Bragg grating center wavelength due to changes in relative humidity (RH) and temperature can be described by²³

$$\frac{\Delta\lambda_B}{\lambda_B} = S_{RH}\Delta RH + S_T\Delta T = [\beta_{cf} - \hat{P}_e(\beta_{cf} - \beta_f)]\Delta RH + [\alpha_{cf} - \hat{P}_e(\alpha_{cf} - \alpha_f) + \zeta]\Delta T, \quad (1)$$

where S_{RH} and S_T are the sensitivities to relative humidity and temperature, respectively. ΔRH and ΔT are the changes in relative humidity and temperature accordingly. β_i is the hygroscopic longitudinal expansion coefficient, which is zero for bare fiber, and α_i is the thermal longitudinal expansion coefficient. The subscript stands for bare fiber ($i=f$) and coated fiber ($i=cf$). ζ is the thermo-optic coefficient of the fiber core and \hat{P}_e is the effective photoelastic coefficient of the coated fiber,²⁴

$$\hat{P}_e = \frac{n^2}{2}[P_{12} - \nu(P_{11} + P_{12})] = 0.213 \quad (2)$$

where P_{11} and P_{12} are the components of the strain-optic tensor, n is the index of refraction of the core, and ν is Poisson's ratio. For a typical optical fiber $P_{11}=0.113$, $P_{12}=0.252$, $n=1.482$, $\nu=0.16$, and $\nu=-\varepsilon_{f,r}/\varepsilon_{f,z}$ where $\varepsilon_{f,r}$ and $\varepsilon_{f,z}$ are the radial and axial elastic fiber strains, respectively.

The temperature sensitivity S_T can thus be obtained

$$S_T = \alpha_{cf} - \hat{P}_e(\alpha_{cf} - \alpha_f) + \zeta. \quad (3)$$

Table I lists some thermo-optic parameters of the fused silica fiber and the polyimide coating. According to the table, the temperature sensitivity can be calculated to be $S_T = (6.70 \pm 0.48) \times 10^{-6} K^{-1}$. The temperature coefficient K_T , defined as $K_T = \Delta\lambda_B/\Delta T$, is $K_T = 0.0104 \text{ nm}/^\circ\text{C}$ at 1550 nm.

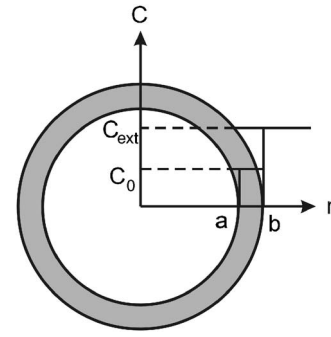


FIG. 1. Schematic illustration of the distribution of the water concentration along the cross section of the fiber.

Since the hygroscopic longitudinal expansion coefficient of the bare fiber (β_f) is zero, the relative humidity sensitivity S_{RH} can be expressed as

$$S_{RH} = (1 - \hat{P}_e)\beta_{cf}. \quad (4)$$

Following the parameters listed in Table I, the relative humidity sensitivity S_{RH} is $1.243 \times 10^{-6} (\%RH^{-1})$. The humidity coefficient K_{RH} , defined as $K_{RH} = \Delta\lambda_B/(\Delta RH)$, is $1.927 \times 10^{-3} \text{ nm}/(\%RH)$ at 1550 nm.

The water accumulation and leakage in the coating material of the FBG is a diffusion process, which can be described by Fick's second law,

$$\frac{\partial c}{\partial t} = D\nabla^2 c, \quad (5)$$

where c is the water concentration, D is the diffusion coefficient, and t is the diffusion time.

For radial diffusion in a cylinder as illustrated in Fig. 1, the general diffusion equation of Eq. (5) can be expressed in cylindrical coordinates

$$\frac{\partial c}{\partial t} = D \frac{1}{r} \frac{\partial}{\partial r} \left(r \frac{\partial c}{\partial r} \right). \quad (6)$$

The boundary condition for the diffusion mass entering the polyimide coating at the position r along the direction of diffusion at time t is

$$c(a < r < b, t = 0) = C_0,$$

$$c(r = b, t \geq 0) = C_{\text{ext}},$$

$$\frac{\partial c}{\partial r}(r = a, t \geq 0) = 0, \quad (7)$$

where C_0 and C_{ext} are the water concentrations corresponding to different radial positions.

When the FBG is immersed in the water bath, the environmental medium can be regarded as a constant concentration source, in which the water outside the fiber will diffuse into the fiber coating until an equilibrium state is reached. The solution of Eq. (6) is

$$c(r, t) = C_{\text{ext}} \operatorname{erf} c \left(\frac{r}{\sqrt{4Dt}} \right). \quad (8)$$

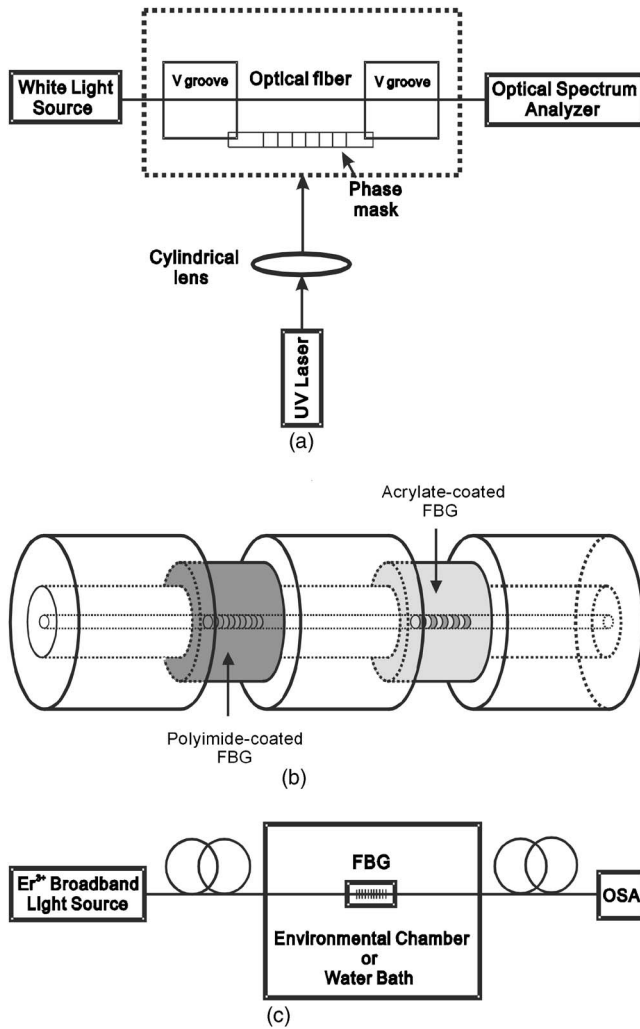


FIG. 2. Multiplexed FBG sensor system and measurement: (a) setup for FBG inscription, (b) illustration of the FBG sensor system used in this study, and (c) experimental setup for the measurement of sensing performance in an environmental chamber or a water bath.

In the case when salt is gradually added into the water bath, the water concentration in the fiber coating will be higher than that in the environmental medium and the water will diffuse into the environmental medium from the fiber coating until an equilibrium state is reached. The solution of Eq. (6) in this case is

$$c(r, t) = C_{\text{ext}} \operatorname{erf}\left(\frac{r}{\sqrt{4Dt}}\right). \quad (9)$$

III. EXPERIMENTAL DETAILS

A standard telecommunication single-mode optical fiber (Corning SMF-28) was soaked in high-pressure hydrogen atmosphere (1900 psi) at room temperature for 2 weeks and then stored in a freezer at -70°C before use. Two FBGs with a grating length of 1 cm for each were inscribed on the hydrogen-loaded fiber using a KrF excimer laser and a phase mask, as illustrated in Fig. 2(a). After the grating fabrication, the FBG sample was baked at 150°C overnight to eliminate the residual hydrogen and the unstable UV-induced index changes. One grating was then recoated with polyimide poly-

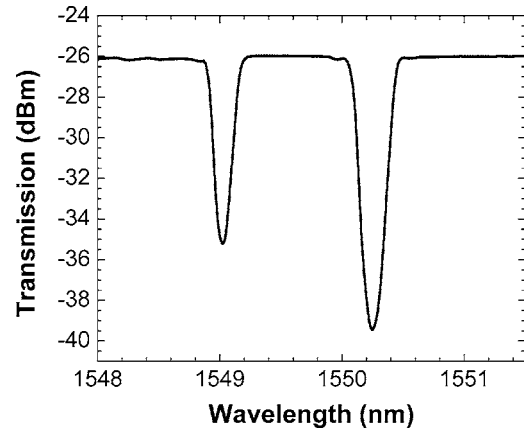


FIG. 3. Transmission spectrum of the FBG sensor system.

mer, while the other one recoated with acrylate polymer. The multiplexed FBG sensor system is shown in Fig. 2(b). The recoating process resulted in a fiber diameter of $173\ \mu\text{m}$ at the grating area. The transmission spectrum of the sensor was measured by an optical spectrum analyzer (Ando 6315E). Figure 3 shows two Bragg wavelengths of the acrylate- and polyimide-coated FBGs at 1549.020 and 1550.244 nm with reflection signals of 9.24 and 13.47 dB, respectively. The characteristics of the multiplexed FBGs are summarized in Table II.

To investigate the temperature responses of the multiplexed FBG sensor in different environments, an environmental chamber and a microcomputer-controlled water bath were used to control the variations of the environmental temperature, in which the air and the water were the corresponding ambient media. Figure 2(c) illustrates the experimental setup used to determine the temperature-induced shift of the FBG transmission spectrum in the environmental chamber or the water bath. When the polymer-coated FBGs had been completely immersed in the water bath, a certain amount of NaCl grains was added into the water to adjust the salinity of the solution. The relationship between the Bragg wavelengths of the multiplexed FBG sensor and the NaCl concentrations of the solutions will be investigated.

IV. RESULTS AND DISCUSSION

A. Temperature measurement

At first, part of the multiplexed FBG sensor with the acrylate-coated grating section was placed in the environ-

TABLE II. Characteristics of the multiplexed sensor system with two polymer-coated FBGs.

Parameter	Acrylate-coated FBG	Polyimide-coated FBG
Fiber type	SMF-28	SMF-28
Fiber recoating type	Acrylate	Polyimide
Physical length (mm)	10	10
Bragg wavelength (air, 20°C) (nm)	1549.020	1550.244
Thickness (μm)	24.1 ± 1.0	24.1 ± 1.0
Bandwidth (nm)	0.170	0.290
Isolation (dB)	8	13
Reflection (%)	90.0	97.2

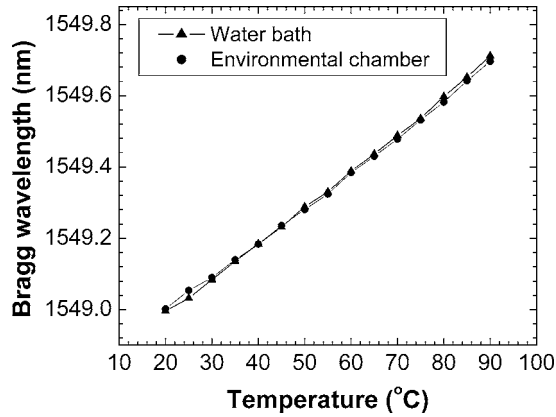


FIG. 4. Bragg wavelength of the acrylate-coated FBG as a function of temperature in the environmental chamber and the water bath.

mental chamber and the FBG was fixed to eliminate the strain or bending cross effects.³⁰ The relative humidity was set at 25%RH to simulate the RH of indoor environment. The initial Bragg wavelength λ_B at a temperature of 20 °C was 1549.002 nm and gradually redshifted with the increasing temperature in the environmental chamber, as shown in Fig. 4. The Bragg wavelength shifted to 1549.696 nm at 90 °C, corresponding to a net shift of 0.694 nm. The temperature coefficient of the acrylate-coated FBG in the air $K_{T_{\text{air}}}$ is 0.0099 nm/°C, which can be obtained from the linear fitting equation $\lambda_B = \lambda_0 + K_{T_{\text{air}}}\Delta T$. During the process of transferring the acrylate-coated FBG from the environmental chamber to the water bath, no apparent shift in the Bragg wavelength was found (Fig. 5). From Fig. 4, the temperature coefficient in water $K_{T_{\text{water}}}$ was measured to be 0.0102 nm/°C, almost the same as $K_{T_{\text{air}}}$. The phenomenon is due to the fact that the acrylate-coated FBG was not sensitive to the change of relative humidity, as indicated in Fig. 6.

Following the same procedure mentioned above, the temperature responses of the polyimide-coated grating of the multiplexed FBG sensor in the air and water were studied separately. In the environmental chamber, the temperature coefficient in the air $K_{T_{\text{air}}}$ was 0.0106 nm/°C, which is shown in Fig. 7. As shown in Fig. 8, the transmission spectra of the polyimide-coated FBG showed the spectral shift to-

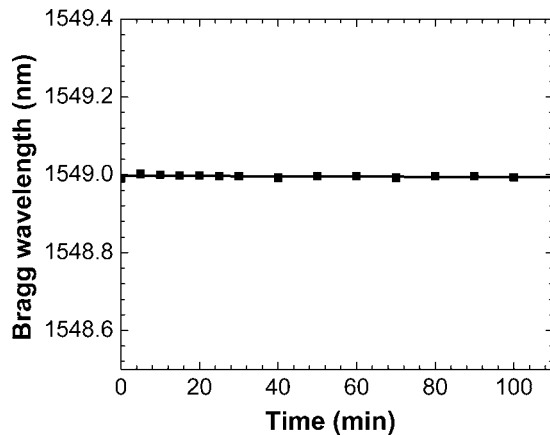


FIG. 5. Time evolution of the shift of the Bragg wavelength of the acrylate-coated FBG.

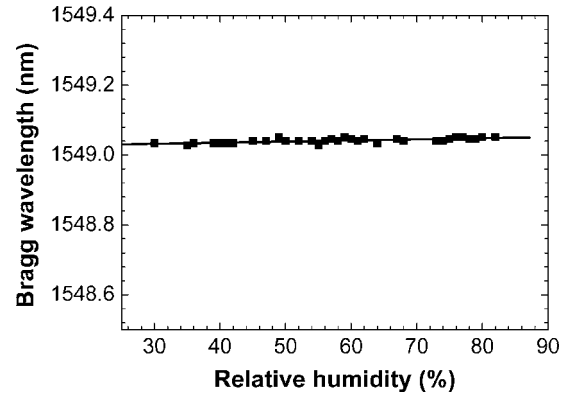


FIG. 6. Bragg wavelength of the acrylate-coated FBG as a function of relative humidity in the environmental chamber at a temperature of 20 °C.

ward longer wavelengths with the increase in the RH, indicating that the polyimide-coated FBG is sensitive to humidity.³¹ The initial FBG resonance wavelength was 1550.192 nm at 13%RH and gradually redshifted with the increase in the relative humidity at a constant temperature of 20 °C in the environmental chamber. The Bragg resonance wavelength shifted to 1550.414 nm at 91%RH corresponding to a shift of 0.222 nm. The dependence of the Bragg wavelength λ_B on the change of the relative humidity ΔRH can be fitted by the equation $\lambda_B = \lambda_0 + K_{RH}\Delta RH$, where K_{RH} is the coefficient of the shift in the resonance wavelength, indicating the effectiveness in changing the resonance wavelength of the FBG by the humidity. In this case, the values of K_{RH} and S_{RH} are 2.846×10^{-3} nm/(%RH) and 1.836×10^{-6} (%RH⁻¹), respectively. Following the same procedures, the K_{RH} values at temperatures of 10, 50, and 80 °C were measured to be 2.615×10^{-3} , 2.500×10^{-3} , and 2.836×10^{-3} nm/(%RH), respectively. For the temperature range of 10–80 °C, the average K_{RH} value of $(2.699 \pm 0.170) \times 10^{-3}$ nm/(%RH) shows a standard deviation of 6.3%, which indicates an excellent linear dependence of the Bragg wavelength on the relative humidity at different temperatures for sensing applications.

The longitudinal expansion coefficients of the coated fiber are the sums of the stiffness-weighted expansion coefficients of the bare fiber and of the coating,²³

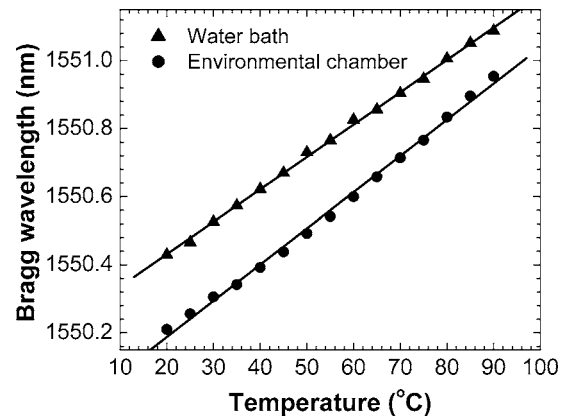


FIG. 7. Bragg wavelength of the polyimide-coated FBG as a function of temperature in the environmental chamber and the water bath.

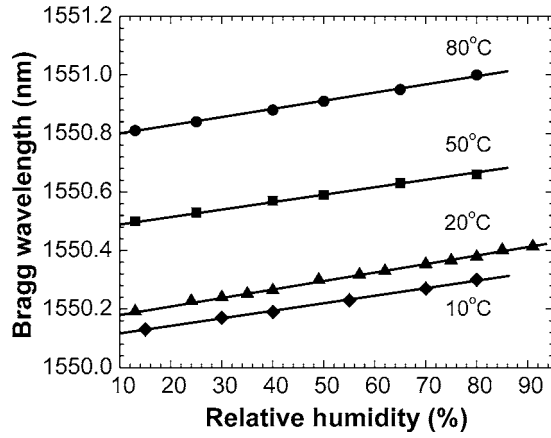


FIG. 8. Bragg wavelength of the polyimide-coated FBG as a function of relative humidity in the environmental chamber at temperatures of 10, 20, 50, and 80 °C.

$$\beta_{cf} = k_f \beta_f + k_c \beta_c, \quad (10)$$

where $k_c = E_c A_c / (E_c A_c + E_f A_f)$ is the stiffness proportion, E_i is Young's modulus, and A_i is the cross-section area.

From the relative humidity sensitivity $S_{RH} = 1.836 \times 10^{-6} (\%RH^{-1})$ together with Eqs. (4) and (10), we have

$$k_c = \frac{\beta_{cf}}{\beta_c} = \frac{S_{RH}}{(1 - \hat{P}_e) \beta_c} = 0.0333. \quad (11)$$

By using the parameters in Table I and the radii of the single-mode fiber and its core, the thickness of the polyimide coating can be calculated to be 26.1 μm from Eq. (10). From an optical microscopy, the thickness of the polyimide coating was observed to be $24.1 \pm 1.0 \mu\text{m}$, indicating a good agreement between the theoretical analyses and the experimental data.

When the polyimide-coated FBG was transferred from the environmental chamber (25%RH) to the water bath at a constant temperature of 20 °C, it was found that the Bragg wavelength redshifted from 1550.218 to 1550.408 nm and stabilized after half an hour (Fig. 9). The polyimide coating absorbed the water and swelled to stretch the fiber. The Bragg wavelength was increasing with a net shift of 0.190 nm due to the expanding grating period, which was caused by the stretched fiber.

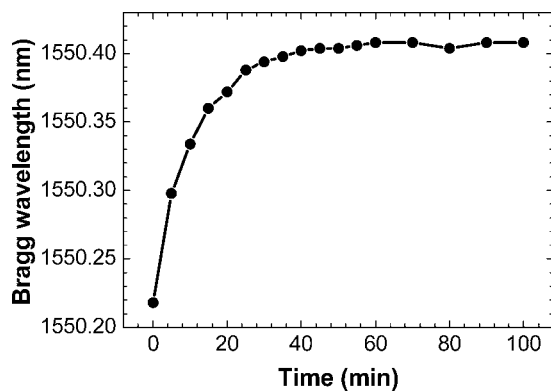


FIG. 9. Time evolution of the shift of the Bragg wavelength of the polyimide-coated FBG.

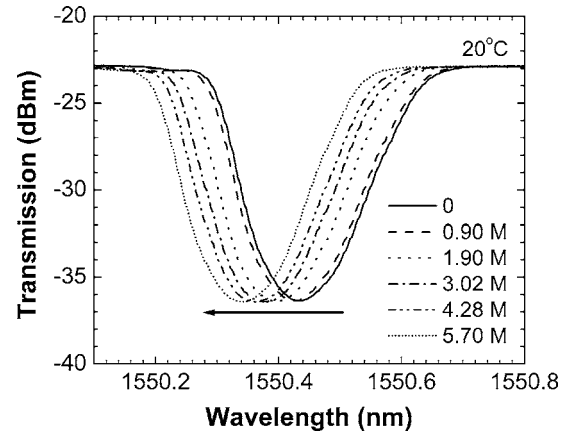


FIG. 10. Transmission spectra of the polyimide-coated FBG at different NaCl concentrations.

In Eq. (8), $D = 10^{-12} \text{ m}^2/\text{s}$,³² $a = 62.5 \mu\text{m}$, $b = 86.6 \mu\text{m}$, and $C_{\text{ext}} = 1$. We consider D is a constant for the fiber coating with a radius between a and b . From Fig. 7, when we take $t = 2400 \text{ s}$, we can obtain

$$c(24.1 \mu\text{m}, t > 2400 \text{ s}) = 0.724 \text{ (W/W \%)}, \quad (12)$$

where W/W% stands for the weight percentage. In the above calculation, we assumed that the layer thickness remains constant, the coating and the fiber interface is impermeable, and the water diffuses perpendicularly to the layer surfaces.

After the transmission spectrum of the polyimide-coated FBG in the water bath is stabilized, the temperature was increased from 20 to 90 °C while the Bragg wavelength redshifted from 1550.430 to 1551.088 nm (Fig. 7). The temperature coefficient of the polyimide-coated FBG in water $K_{T_{\text{water}}}$ was 0.0094 nm/°C, which is similar to its temperature coefficient in the air. Figure 7 indicates that the Bragg wavelength difference between the two cases when the grating was stored in either the environmental chamber or the water bath is decreasing with the increase in temperature from 0.220 nm at 20 °C to 0.134 nm at 90 °C. This is mainly due to the reduced hydrophilic capability of the polyimide coating near the water boiling point.

B. Salinity measurement

After both of the polyimide- and acrylate-coated FBGs were completely immersed in the water bath for half an hour and kept the water temperature stable at 20 °C, a certain amount of NaCl grains was added into the water to produce desired solutions of different degrees of salinity with the NaCl concentration ranging from 0 to 5.70 mol/l. The transmission spectra of the polyimide-coated FBG at different NaCl concentrations are shown in Fig. 10. When the NaCl grains were added into the water bath, the water concentration around the grating decreased, which resulted in the decrease of the corresponding water concentration in the polyimide coating. In our experiment, for each time the NaCl grains were added, sufficient waiting time was observed to make the FBG spectrum immovable and the stabilization time was recorded.

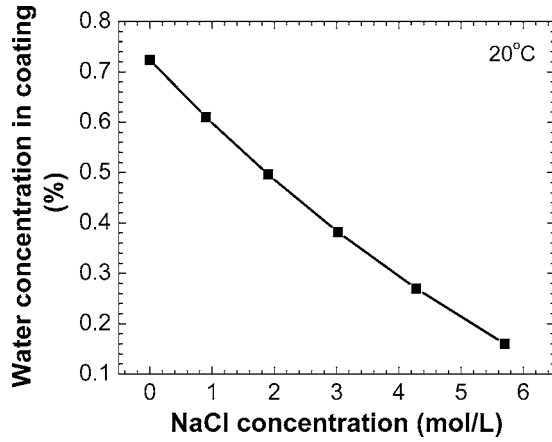


FIG. 11. The relationship between the water concentration in the coating of the polyimide-coated FBG and the ambient NaCl concentration.

According to Eq. (9), the water concentration in the coating of the polyimide-coated FBG in different solutions can be calculated. For the external NaCl concentration gradually increased from 0 to 5.70 mol/l, as shown in Fig. 10, the diffusion stabilization times t were 140, 165, 200, 260, and 410 s, respectively. Figure 11 shows the relationship between the water concentration in the coating of the polyimide-coated grating and the external NaCl concentration. The decreasing diffusion stability time leads to less change in the water concentration in the coating material.

Figure 12 shows the Bragg wavelengths of the two FBGs as functions of NaCl concentrations. It shows that the sensitivity of the polyimide-coated FBG on salinity is 0.0165 nm/M. The figure also indicates that the shrinkage of the polyimide coating in NaCl solutions resulted in the blue-shift of the Bragg wavelength of the polyimide-coated FBG. However, the acrylate-coated FBG was not sensitive to the change of salinity in the NaCl solution. We define a character matrix M_{TS} to represent the sensing performance of the multiplexed sensor,

$$\begin{bmatrix} \Delta\lambda_1 \\ \Delta\lambda_2 \end{bmatrix} = M_{TS} \begin{bmatrix} \Delta T \\ \Delta M \end{bmatrix}. \quad (13)$$

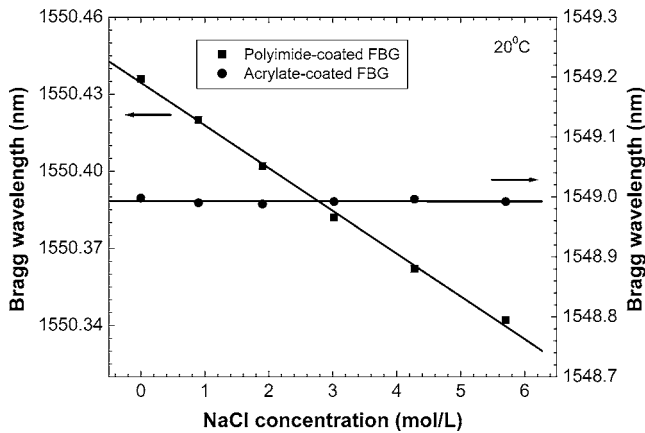


FIG. 12. Bragg wavelengths of acrylate- and polyimide-coated FBGs as functions of NaCl concentrations.

In this particular case, the character matrix M_{TS} can be used to determine the variations in the salinity of water and its temperature from the readings of the wavelength shifts of the two gratings,

$$\begin{bmatrix} \Delta\lambda_1 \\ \Delta\lambda_2 \end{bmatrix} = \begin{bmatrix} 0.0102 & 0 \\ 0.0094 & -0.0165 \end{bmatrix} \begin{bmatrix} \Delta T \\ \Delta M \end{bmatrix}, \quad (14)$$

where $\Delta\lambda_1$ and $\Delta\lambda_2$ correspond to the shifts in the Bragg wavelengths of the acrylate- and polyimide-coated FBGs, respectively.

This scheme offers a number of advantages over other reported methods of salinity measurement. With this multiplexed FBG sensor, it is possible to measure the salinity through the polyimide-coated FBG while simultaneously determine the temperature with the acrylate-coated FBG. In addition, though only two FBGs of Bragg wavelengths at 1549.020 and 1550.244 nm were adopted in this study, it is possible to introduce more wavelength channels to realize quasidistributed salinity measurement. Furthermore, the FBG fabrication process and the recoating technique are quite simple, which is promising to realize low-cost salinity sensors.

V. CONCLUSION

In summary, a new technique for simultaneous measurement of temperature and salinity has been discussed. The proposed in-line one-fiber sensor system consists of FBGs coated by different polymers with the acrylate-coated one sensitive to the temperature only while the polyimide-coated one monitoring the salinity. The experimental results demonstrated that the temperature sensitivity of the acrylate-coated grating in water was 0.0102 nm/°C for redshifted Bragg wavelength with increasing temperature, and the temperature and the salinity sensitivities of the polyimide-coated grating were 0.0094 nm/°C (redshifted) and 0.0165 nm/M (blue-shifted), respectively, which are in excellent agreement with the theoretical analysis. Compared with all reported optical techniques to realize salinity measurement, the approach proposed here is the simplest in the configuration and fabrication of a transducer while accurate salinity and temperature measurement are realized without resorting to empirical algorithms. This approach also offers the possibility to introduce more wavelength channels to realize a quasidistributed measurement. Since the two sensing elements have been integrated on one standard single-mode telecommunication fiber, it is possible to achieve quasidistributed *in situ* measurement of temperature and salinity over a long distance.

ACKNOWLEDGMENTS

The authors thank Natural Sciences and Engineering Research Council of Canada (NSERC) for the grant support to this research project. One of the authors (Q.C.) thanks Canada Research Chairs Program, Canada Foundation for Innovation, the Province of Newfoundland and Labrador, and the Memorial University of Newfoundland on the support of research infrastructure.

¹Salinity: *Environment—Plants—Molecules*, edited by A. Läuchli and U.

- Lüttge (Springer, Dordrecht, 2002).
- ²Ocean Weather Forecasting: *An Integrated View of Oceanography*, edited by E. P. Chassignet and J. Verron (Springer, Dordrecht, 2006).
- ³O. Esteban, M. Cruz-Navarrete, A. González-Cano, and E. Bernabeu, *Appl. Opt.* **38**, 5267 (1999).
- ⁴M. Born and E. Wolf, *Principles of Optics*, 7th ed. (Cambridge University Press, Cambridge, 2005).
- ⁵M. Cervantes and R. Rodriguez-Vera, *Appl. Opt.* **27**, 4494 (1988).
- ⁶Y.-L. Lo and C.-H. Chuang, *Appl. Opt.* **40**, 3518 (2001).
- ⁷G. J. Veldhuis and P. V. Lambeck, *Appl. Phys. Lett.* **71**, 2895 (1997).
- ⁸Y. Zhao and Y. Liao, *Sens. Actuators B* **86**, 63 (2002).
- ⁹Y. Zhao, Y. Liao, B. Zhang, and S. Lai, *J. Lightwave Technol.* **21**, 1334 (2003).
- ¹⁰*Handbook of Optical Fibre Sensing Technology*, edited by J. M. López-Higuera (Wiley, West Sussex, 2002).
- ¹¹M. G. Kuzyk, *Polymer Fiber Optics: Materials, Physics, and Applications* (CRC, Boca Raton, FL, 2006).
- ¹²S. Sade and A. Katzir, *J. Appl. Phys.* **96**, 3507 (2004).
- ¹³C. Zhang, W. Li, X. Bao, L. Chen, and M. Du, *Opt. Lett.* **32**, 2565 (2007).
- ¹⁴E. Shafir, G. Berkovic, Y. Horovitz, G. Appelbaum, E. Moshe, E. Horovitz, A. Skutelski, M. Werdiger, L. Perelmutter, and M. Sudai, *J. Appl. Phys.* **101**, 093107 (2007).
- ¹⁵J. Weng, H. Tan, X. Wang, Y. Ma, S. Hu, and X. Wang, *Appl. Phys. Lett.* **89**, 111101 (2006).
- ¹⁶A. Cusano, M. Consales, A. Cutolo, M. Penza, P. Aversa, M. Giordano, and A. Guemes, *Appl. Phys. Lett.* **89**, 201106 (2006).
- ¹⁷B. McMillen, C. Jewart, M. Buric, K. P. Chen, Y. Lin, and W. Xu, *Appl. Phys. Lett.* **87**, 234101 (2005).
- ¹⁸A. K. Sharma and B. D. Gupta, *J. Appl. Phys.* **101**, 093111 (2007).
- ¹⁹S. Rengarajan and R. M. Walser, *J. Appl. Phys.* **81**, 4278 (1997).
- ²⁰D. J. Gentleman and K. S. Booksh, *Talanta* **68**, 504 (2006).
- ²¹R. Falate, O. Frazão, G. Rego, J. L. Fabris, and J. L. Santos, *Appl. Opt.* **45**, 5066 (2006).
- ²²J. Cong, X. Zhang, K. Chen, and J. Xu, *Sens. Actuators B* **87**, 487 (2002).
- ²³P. Kronenberg, P. K. Rastogi, P. Giaccari, and H. G. Limberger, *Opt. Lett.* **27**, 1385 (2002).
- ²⁴G. Meltz and W. W. Morey, *Proc. SPIE* **1516**, 185 (1991).
- ²⁵G. B. Hocker, *Appl. Opt.* **18**, 1445 (1979).
- ²⁶“Pyralin Product Information,” HD MicroSystems, 2001.
- ²⁷A. T. Alavie, R. Maaskant, R. Stubbe, A. Othonos, M. Ohn, B. Sahlgren, and R. M. Measures, *Proc. SPIE* **2444**, 528 (1995).
- ²⁸F. P. Mallinder and B. A. Proctor, *Phys. Chem. Glasses* **5**, 91 (1964).
- ²⁹K. Sager, A. Schroth, A. Nakladal, and G. Gerlach, *Sens. Actuators, A* **53**, 330 (1996).
- ³⁰N. Mohammad, W. Szyszowski, W. J. Zhang, E. I. Haddad, J. Zou, W. Jamroz, and R. Kruselecky, *J. Lightwave Technol.* **22**, 2001 (2004).
- ³¹T. L. Yeo, T. Sun, K. T. V. Grattan, D. Parry, R. Lade, and B. D. Powell, *IEEE Sens. J.* **5**, 1082 (2005).
- ³²J. L. Mrotek, M. J. Matthewson, and C. R. Kurkjian, *J. Lightwave Technol.* **19**, 988 (2001).